Protein exchange dynamics at chemoreceptor clusters in *Escherichia coli*

Sonja Schulmeister[†], Michaela Ruttorf[‡], Sebastian Thiem[†], David Kentner[†], Dirk Lebiedz[§], and Victor Sourjik[†¶]

[†]Zentrum für Molekulare Biologie and [‡]Interdisziplinäres Zentrum für Wissenschaftliches Rechnen, Universität Heidelberg, D-69120 Heidelberg, Germany; and [§]Zentrum für Biosystemanalyse, Universität Freiburg, Schänzlestrasse 1, D-79104 Freiburg, Germany

Edited by Sung-Hou Kim, University of California, Berkeley, CA, and approved February 28, 2008 (received for review November 8, 2007)

Signal processing in bacterial chemotaxis relies on large sensory complexes consisting of thousands of protein molecules. These clusters create a scaffold that increases the efficiency of pathway reactions and amplifies and integrates chemotactic signals. The cluster core in *Escherichia coli* comprises a ternary complex composed of receptors, kinase CheA, and adaptor protein CheW. All other chemotaxis proteins localize to clusters by binding either directly to receptors or to CheA. Here, we used fluorescence recovery after photobleaching (FRAP) to investigate the turnover of chemotaxis proteins at the cluster and their mobility in the cytoplasm. We found that cluster exchange kinetics were protein-specific and took place on several characteristic time scales that correspond to excitation, adaptation, and cell division, respectively. We further applied analytical and numerical data fitting to analyze intracellular protein diffusion and to estimate the rate constants of cluster equilibration *in vivo*. Our results indicate that the rates of protein turnover at the cluster have evolved to ensure optimal performance of the chemotaxis pathway.

bacteria | chemotaxis | diffusion | FRAP | signal transduction

The relatively simple chemotaxis signaling pathway in *Escherichia coli*, with analogues of its components—receptors, kinase, phosphatase, and adaptation system—common to many other networks, is an ideal model system for studying general principles of signal transduction (1–3). In *E. coli*, allosteric interactions among receptors in chemosensory arrays or clusters (Fig. 1), where receptors of different ligand specificities are intermixed (4, 5), integrate and amplify chemotactic stimuli. The networked receptors regulate the autophosphorylation activity of an associated kinase, CheA, which in turn controls the phosphorylation state of a small response regulator protein, CheY, to modulate the cell's flagellar motors. The signaling pathway also includes CheZ, a phosphatase of CheY-P. Excitatory signaling is rapid: changes in CheY phosphorylation level upon repellent or attractant stimulation take place in several hundreds of milliseconds (6–9).

In addition, the pathway includes an adaptation system, comprising methyltransferase CheR and methylesterase CheB, that adjusts the activity and sensitivity of the sensory complex by methylating and demethylating receptors. The adaptation system uses feedback from receptor and kinase activity to return CheY phosphorylation to a preset level even in the presence of high levels of chemoeffectors. The time course of the adaptation process depends on stimulus strength (10, 11), varying from several seconds for weak stimuli to several minutes for strong stimuli.

Most of the reaction rates and binding constants for chemotaxis proteins have been measured *in vitro*, and the average intracellular protein concentrations under standard growth conditions were determined (12, 13). This abundance of biochemical data has inspired multiple attempts at detailed kinetic analysis of the chemotaxis pathway (9, 13–17), making it the most thoroughly modeled signaling pathway in biology.

One of the open questions in a quantitative understanding of the pathway is the role of spatial organization in chemotactic signaling. With few exceptions (18), current computer models of chemotaxis do not take into account its spatial aspects, even though receptor clustering occurs in all studied bacterial chemotaxis systems. Spatiotemporal modeling of intracellular processes is a generally challenging task because of the crowded and nonhomogeneous nature of the cytoplasm (19). However, several modeling approaches have been recently developed (20–22), and the main limitation at this stage is a lack of quantitative information on the intracellular mobility and exchange kinetics of signaling proteins at the macromolecular complexes. To acquire a comprehensive set of such data for *E. coli* chemotaxis, we applied fluorescence recovery after photobleaching (FRAP) to a library of yellow fluorescent protein (YFP) fusions to all

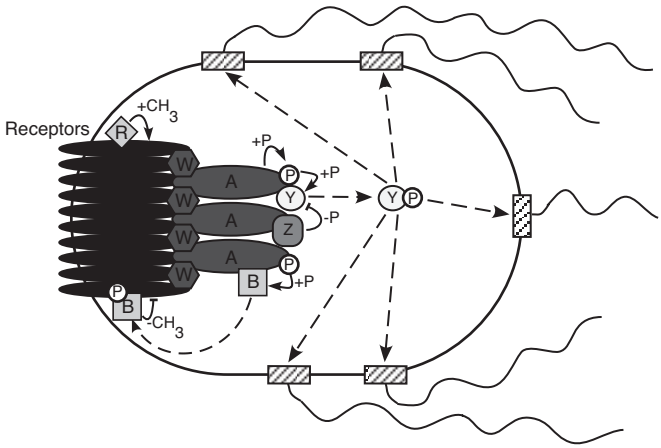

Fig. 1. Schematic representation of the chemotaxis pathway. Chemotactic stimuli are sensed by membrane clusters that consist of receptors and associated chemotaxis proteins, of which only CheA and CheW are important for clustering. CheA autophosphorylates in a stimulation-dependent manner and transfers the phosphate group to either CheY or CheB, which share a common binding site on CheA. Phosphorylated CheY is either dephosphorylated by CheZ, which associates with clusters via binding to CheA, or is released into the cytoplasm where it can regulate the rotation of flagellar motors. CheR and CheB bind to the C terminus of receptors and add or remove, respectively, methyl groups on specific glutamate residues; CheB activity is enhanced by phosphorylation. Grayscale indicates stability of protein association with clusters as determined in this study, with darker shading corresponding to more stable association.

Author contributions: V.S. designed research; S.S., M.R., S.T., and V.S. performed research; S.S., M.R., D.K., and V.S. contributed new reagents/analytic tools; S.S., M.R., D.L., and V.S. analyzed data; and S.S., M.R., and V.S. wrote the paper.

The authors declare no conflict of interest.

This article is a PNAS Direct Submission.

¶To whom correspondence should be addressed at: Zentrum für Molekulare Biologie der Universität Heidelberg, Im Neuenheimer Feld 282, D-69120 Heidelberg, Germany. E-mail: v.sourjik@zmbh.uni-heidelberg.de.

This article contains supporting information online at www.pnas.org/cgi/content/full/0710611105/DCSupplemental.

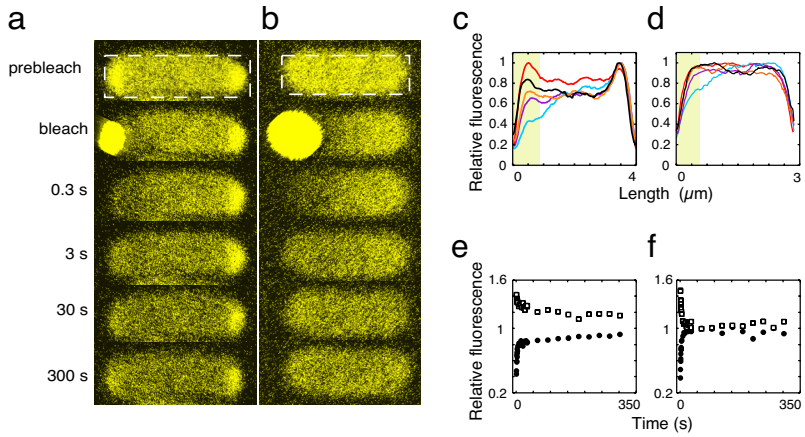

Fig. 2. Sample FRAP measurement. (*a* and *b*) FRAP sequences of a CheZ-YFP fusion, expressed in VS102 (Δ*flgM*) (*a*) and in VS116 (Δ*flhC*) (*b*) strains. After a prebleach image was acquired, the polar region in each sequence was bleached by two high-intensity laser scans (second frame). Recovery of fluorescence was followed for 300 s; only selected images are shown. (*c* and *d*) Corresponding fluorescence intensity profiles for VS102 (*c*) and VS116 (*d*) cells were measured within a stripe drawn over the entire cell length as described in *Methods* in the prebleach image (red) and in the images that were taken 0.3 s (blue), 3 s (purple), 30 s (orange), and 300 s (black) after bleaching. To facilitate comparison, smoothed intensity profiles were normalized to the maximal intensity value. The evaluated region is highlightened in yellow. (*e* and *f*) Recovery of fluorescence in the evaluated bleached region (filled circles) and loss of fluorescence in the unbleached (open squares) region in VS102 (*e*) and VS116 (*f*) cells over time. Fluorescence intensity in the region of interest was normalized to intensity of the entire cell and then again to the normalized intensity in the prebleach image. See *Methods* for details of experiments and data analysis.

cytoplasmic chemotaxis proteins and to the aspartate receptor Tar and derived rate constants for protein diffusion and exchange at the cluster from the recovery curves.

Results

Measurements of Protein Mobility and Exchange at the Cluster. In a typical FRAP experiment, we bleached fluorescence of a YFP fusion protein of interest (e.g., CheZ-YFP; Fig. 2) in the polar region of a cell and subsequently followed the recovery of fluorescence in that region by taking a series of images at varying time intervals. To facilitate data analysis, the fluorescence intensity in the region of interest (ROI) was normalized to the fluorescence of the entire cell at each time point; these ratio values were subsequently renormalized to the prebleach ratio (see *Methods* for details). Because of the limited resolution of fluorescence microscopy and the small size of bacterial cells, we always bleached a larger fraction of the cell volume than that occupied by a receptor cluster (Fig. 2 *a* and *c*). Consequently, the kinetics of fluorescence recovery in the cells that contained receptor clusters showed two phases: the initial fast recovery, which resulted from a diffusion-driven exchange of the fluorescent proteins in the cytoplasm, followed by a slower exchange between cluster-bound and cytoplasmic proteins (Fig. 2 *a*, *c*, and *e*). In a cell without clusters, only the fast diffusional phase was observed (Fig. 2 *b*, *d*, and *f*). In both cases, the relative fluorescence saturated around a value of one after recovery (Fig. 2 *e* and *f*), meaning that the proteins were largely equilibrated. To better separate the cluster exchange kinetics from diffusion, we performed our experiments in two different background strains, VS102 (Δ*flgM*) and VS116 (Δ*flhC*). The former has a functional chemotaxis system and correct protein stoichiometry but with average protein levels approximately sixfold above normal (15), which leads to formation of larger receptor clusters and facilitates FRAP measurements (Fig. 2*a*). The latter does not express any chemotaxis proteins and completely lacks clusters (Fig. 2*b*).

We applied this FRAP approach to analyze the mobility and cluster dynamics of YFP fusions to all cytoplasmic chemotaxis proteins and the aspartate receptor Tar. In our preliminary experiments, similar recovery kinetics were observed for the C- and N-terminal YFP fusions to the same protein (data not shown), and only the former were analyzed in greater detail (Fig. 3). The exception was CheA, where an N-terminal fusion to a truncated protein lacking the first two CheA domains, YFP-CheA$^{\Delta 258}$, showed the best localization and was therefore used for detailed analysis. Except for CheY, the recovery kinetics of chemotaxis proteins at the cluster could be well separated from their diffusional exchange in the cytoplasm or in the membrane, as evidenced by comparison of the recovery curves for strains VS102 and VS116 (Fig. 3 *b*–*g*, filled and open symbols, respectively). The decrease in fluorescence at the unbleached side of the cell was used as a control and always followed the same time course as fluorescence recovery at the bleached side (Fig. 3 *Insets*).

Diffusional Exchange of Chemotaxis Proteins. The kinetics of diffusional recovery in the VS116 background fitted well to a function (Eq. **1** in *Methods*) proposed in ref. 23, which takes into account the possibility of anomalous diffusion (see below) by including the parameter α. The estimated values of the half-time for diffusional recovery ($t_{1/2}$) were used to calculate the effective diffusion coefficient of a free protein, using the relation $D \approx 0.07L^2/t_{1/2}$ (24, 25), where L is the cell length. The values of diffusion coefficients estimated this way were validated by fitting the data with a numerically simulated model of protein diffusion [Table 1; see *Methods* and supporting information (SI) *Text* for modeling and simulation details]. As expected, there was, on average, an inverse correlation between the size of a protein and its estimated diffusion coefficient, and the recovery for the transmembrane Tar-YFP was much slower than for cytoplasmic proteins. However, the experimental recovery curves in VS116 cells, where diffusion should be the only recovery factor, could not be fitted well by using a standard diffusion model (Fig. S1). These results indicate that both cytoplasmic and membrane proteins undergo anomalous rather than normal diffusion. Such anomalous diffusion, with the mean squared displacement of a protein growing less than linear in time, was described in refs. 19, 23, 24, 26, and 27 and is believed to be due to the inhomogeneous viscosity of the cytoplasm and the cell membrane. Following an approach developed in refs. 28–30, we used the concept of binding to ghost particles to describe anomalous diffusion, which

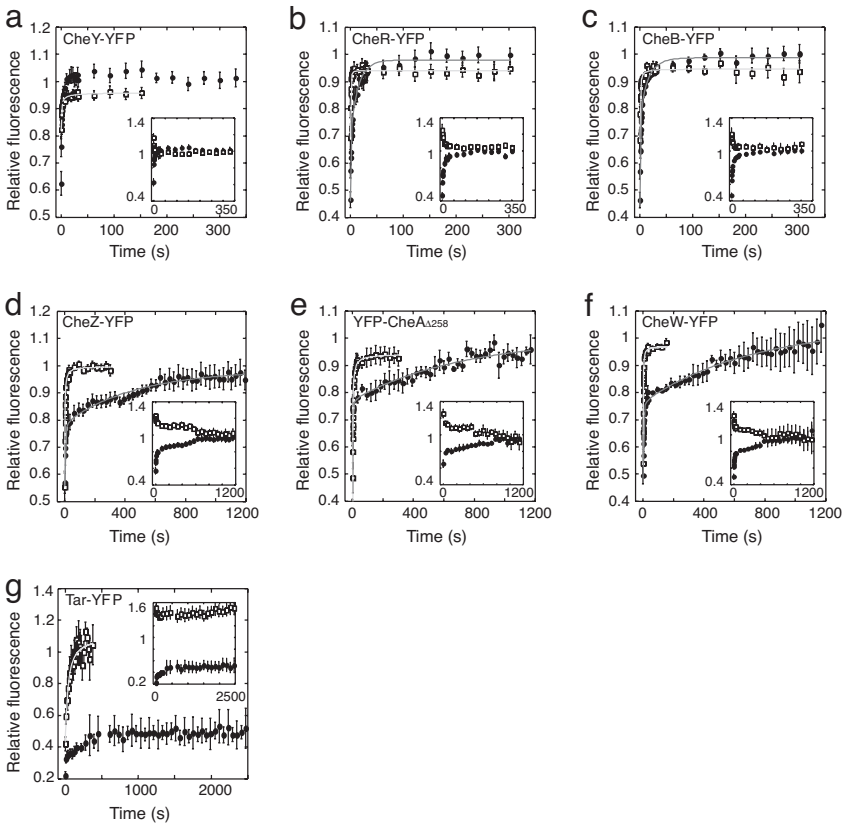

Fig. 3. Recovery curves for chemotaxis protein fusions. Kinetics of fluorescence recovery in the bleached regions for YFP fusions to CheY (*a*), CheB (*b*), CheR (*c*), CheZ (*d*), CheA$^{\Delta 258}$ (*e*), CheW (*f*), and Tar (*g*) in VS102 (filled circles) and in VS116 (open squares). The kinetics are means of 7 to 20 experiments; error bars indicate standard errors. Solid lines are fits to the VS116 data, using Eq. **1** (light gray), and to the VS102 data, using Eq. **2** (dark gray); see *Methods* for details. (*Insets*) Comparison of fluorescence recovery at the bleached cluster (filled circles) and fluorescence loss at the unbleached cluster (open squares) in the same VS102 cells.

proved to be effective in fitting recovery curves in VS116 cells (Fig. S1).

Exchange of Proteins at the Cluster. Rates of fluorescence recovery at clusters in VS102 cells were determined by a diffusional component and an interaction component. The latter is characterized by the off-rate constants k_{off} and the pseudo-first-order on-rate constant $^*k_{on} = k_{on}S$, where k_{on} is the microscopic on-rate constant, and S is the number of available binding sites at the cluster (31). When protein binding is much slower than diffusion (i.e., exchange at the cluster is reaction-dominated), the overall recovery kinetics can be clearly separated in two phases, with the binding part being approximated by an exponential decay (31, 32). The criterion for such separation can be expressed as $(^*k_{on}w^2/D) \ll 1$, where w is the size of the bleached spot (31), and is fulfilled for all cytoplasmic protein fusions except CheY (Table 1). The resulting function that

Table 1. Diffusion and binding parameters of protein fusions.

Protein fusion	Molecular mass, kDa	$t_{1/2}$, s[†]	D_a, $\mu m^2 s^{-1}$[‡]	D_n, $\mu m^2 s^{-1}$[§]	F[¶]	C	τ_{obs}, s[‖]	k_{off}, s^{-1}[††]	$^*k_{on}w^2/D$[‡‡]
CheY-YFP	40.660	0.61 ± 0.12	1.26 ± 0.22	1.32 ± 0.65	n.d.	n.d.	n.d.	0.17 ± 0.11[d]	n.d.
CheW-YFP	44.780	0.89 ± 0.04	0.86 ± 0.03	0.74 ± 0.1	0.29	0.28	723.8 ± 111.0	0.0014 ± 0.0002	0.0009
CheR-YFP	59.550	0.40 ± 0.04	1.89 ± 0.17	1.22 ± 0.44	0.24	0.28	14.7 ± 1.7	0.068 ± 0.008	0.023
CheB-YFP	64.170	0.56 ± 0.08	1.36 ± 0.18	1.39 ± 0.43	0.36	0.18	16.3 ± 1.7	0.061 ± 0.007	0.013
CheZ-YFP	101.35[§§]	1.16 ± 0.06	0.66 ± 0.03	0.56 ± 0.1	0.25	0.19	465.7 ± 56.5	0.0022 ± 0.0003	0.003
YFP-CheA$^{\Delta 258}$	139.17[§§]	1.21 ± 0.05	0.63 ± 0.02	0.37 ± 0.05	0.12	0.23	747.7 ± 236.9	0.0013 ± 0.0005	0.002
Tar-YFP	173.28[§§]	42.3 ± 5.7	0.018 ± 0.002	n.d.	n.d.	n.d.	n.d.	n.d.	n.d.

[†]Estimated from the fit of Eq. **1** to the recovery data for VS116 cells.
[‡]Analytical estimation of diffusion coefficient, calculated as $0.07L^2/t_{1/2}$ for $L = 3.3$ μm.
[§]Numerical estimation of diffusion coefficient (see *Methods*).
[¶]Value of F might be underestimated, because, due to the limited time resolution of the confocal microscope (0.336 s), some recovery of the free protein occurs already before the first measurement point.
[‖]Estimated from the fit of Eq. **2** to the recovery data for VS102 cells.
[††]Calculated as τ_{obs}^{-1}.
[‡‡]Calculated as $k_{off}C/F(0.75)^2/D_a$.
[§§]Calculated for a dimer.

combines both exchange components (Eq. **2** in *Methods*) was used to fit the recovery in the VS102 background, with the values of $t_{1/2}$ and α substituted from the fits to the VS116 data. The values of τ_{obs} derived from the fit to Eq. **2** characterize the turnover rate of the bound protein at the cluster, whereas the amplitudes of the fast and slow recovery phases, F and C, reflect the steady-state concentrations of free and bound protein, respectively (Table 1). As shown in *SI Text*, τ_{obs} can be used to estimate the off-rate of protein dissociation from the cluster as $k_{off} \approx \tau_{obs}^{-1}$ (31, 32). The pseudo-first-order on-rate can be estimated as $^*k_{on} = k_{off}C/F$ (31).

The characteristic exchange time τ_{obs} and the derived values of k_{off} fell into several classes (Table 1). CheY showed very fast recovery on the time scale of several seconds, which could not be clearly resolved from the recovery of the cytoplasmic fraction. In this case, the recovery could not be fitted by Eq. **2**, and we used a numerical model simulation that incorporates anomalous diffusion and binding to estimate the value for k_{off}. For CheB and CheR, recovery took ≈15 seconds; CheZ, CheA, and CheW showed slow recovery that took 5–10 minutes. For Tar, only a partial recovery was observed, with a large fraction of protein remaining immobile on the time scale of half an hour. In contrast, the relative fractions of bound and unbound protein showed similar values for all fusions except for CheY, where it could not be determined (Table 1).

Discussion

Mobility of YFP Fusions to Chemotaxis Proteins. On average, the mobility of cytoplasmic proteins showed the expected inverse correlation between size (i.e., molecular weight) and estimated diffusion coefficient (Table 1). Cytoplasmic exchange was relatively fast: Even the largest proteins equilibrated with half-times of <1.5 s, comparable to the excitation time scale of chemotactic signaling. Numerical data fitting further suggested that cytoplasmic exchange of proteins could not be described by a simple effective diffusion even in absence of cluster formation (Fig. S1). Such anomalous mobility has been recently described in bacteria (19, 24) and in eukaryotes (23, 27) and implies that, on the time scale of our measurements, the motion of a protein is dominated by collisions with surrounding obstacles. In bacteria, which lack the extensive network of cytoskeletal filaments, such diffusive behavior is likely due to molecular crowding, the high density of macromolecules in the cytoplasm and in the inner membrane (19, 27).

Single molecule tracking has been used recently to determine diffusion coefficients for YFP fusions to several proteins in *Caulobacter crescentus*. The diffusion coefficient of 0.012 $\mu m^2 s^{-1}$ measured for a 117-kDa membrane protein PleC-YFP with four membrane-spanning domains (33) was very similar to our estimate of 0.018 $\mu m^2 \cdot s^{-1}$ for the Tar-YFP dimer (173 kDa). The diffusion coefficient for another *E. coli* membrane protein, GFP-MotB (122 kDa), was estimated to be two times smaller, 0.008 $\mu m^2 \cdot s^{-1}$ (35). However, the diffusion of MotB might be slower than expected because the protein can transiently associate with the cell wall. The reported values of 1.1–1.8 $\mu m^2\ s^{-1}$ for a 62-kDa cytoplasmic protein MreB-YFP (34) are in the same range as the values of 1.2–1.9 $\mu m^2 \cdot s^{-1}$ for the similarly sized CheR-YFP (60 kDa) and CheB-YFP (64 kDa). A different technique, fluorescence correlation spectroscopy (FCS), was used to measure the diffusion coefficient of CheY-GFP in *E. coli* as 4.6 $\mu m^2 \cdot s^{-1}$ (36), which is several times higher than our estimate. The discrepancy can be attributed to the difference in the measurement techniques, with FRAP analysis underestimating the rapidly diffusing fraction of a protein because of the small size of bacterial cells and the limited time resolution of a FRAP experiment (0.33 s), and with FCS missing a slowly diffusing fraction.

Multiple Time Scales of Protein Exchange at a Cluster. Measured turnover times enabled us to distinguish several classes of proteins bound to the sensory cluster (Fig. 1). Receptors form a stable core for the cluster. Its extremely high stability—longer than a cell generation—may be explained by multiple interactions among receptors and with CheA and CheW, which hold receptors together within the cluster. CheW and CheA also exchange slowly, but faster than receptors; the observed characteristic time of ≈12 min agrees well with published *in vitro* data (37). The receptor–CheW–CheA complex is therefore stable on the time scale of response and adaptation. With the exchange time of ≈8 min, CheZ can be considered a further part of the stable cluster core. Such stable association of the phosphatase with the cluster presumably helps to prevent formation of a CheY-P gradient in the cytoplasm (9, 38). The residual slow exchange of the cytoplasmic cluster components might be beneficial to ensure that all sensory complexes in the cell have similar stoichiometry, which might be important because the ratio of receptors to CheW to CheA has been shown to affect the regulation of kinase activity by receptors (4).

CheR and CheB enzymes that participate in adaptation represent the next level of stability. Their equilibration times of ≈15 s are substantially longer than the characteristic response (excitation) time of the chemotaxis system (≈0.1–1 s) (6–9) or the typical run time of an adapted swimming cell (≈2 s) (39) but are comparable with the time required for adaptation to saturating stimuli (10, 11). Equilibration on this time scale would ensure a uniform distribution of adaptation enzymes in a cluster and between multiple clusters in the same cell and might be particularly important because of the low copy numbers of CheR and CheB in the cell (200–400), compared with ≈15,000 receptors and 3,000–8,000 copies of all other cytoplasmic proteins (12). Low ration of adaptation enzymes to receptors implies that they have to move around the cluster during the adaptation process to sample all available methylation sites (40). However, the dwell time of CheR and CheB has to be long enough to allow slow adaptation kinetics. Notably, the observed equilibration time of the adaptation enzymes matches well the correlation time of observed slow fluctuations in the bias of flagellar motors (41). Such fluctuations are believed to be important for optimizing bacterial search behavior. Our results support the idea that these fluctuations arise from the stochastic binding and unbinding of CheR and CheB at the cluster (41).

CheY is the only protein that showed rapid exchange kinetics on the signaling time scale, which is consistent with its role as messenger between the spatially localized sensory clusters and flagellar motors. Indeed, previous analysis suggested that the response rate in chemotaxis might be limited by the diffusion of CheY, rather than by its dissociation or phosphotransfer rate (9).

It was proposed that multivalent chemotaxis proteins—receptors, CheA, CheR, CheB, CheZ—can move two-dimensionally along the cluster without dissociation, through consecutive unbinding and reattachment of individual domains, or molecular brachiation (40). In our experiments, however, the recovery kinetics upon bleaching of only a part of the cluster were similar to those for the whole-cluster bleaching (data not shown), suggesting that the exchange of all of these proteins takes place primarily through equilibration with the cytoplasmic (or membrane) pool.

The exchange rates in our work were determined for non-growing adapted cells, under conditions that are used for most quantitative chemotaxis experiments and typically described by computer models. However, the stability of the receptor cluster is likely to be affected by the signaling and adaptation state of the pathway, with changes in ligand binding and protein methylation or phopshorylation influencing not only proteins' conformations but also rate constants of their binding and dissociation. Indeed, the assembly rate of the cluster core was shown to

depend on the state of receptor modification *in vitro* (42). Such dependence could potentially allow regulation of protein stoichiometry and the size of receptor clusters in response to stimulation and thereby play an important role in signaling.

In conclusion, in this work, we systematically mapped *in vivo* dynamics of chemosensory clusters in *E. coli*. Taken together, our results fill one of the last gaps in a quantitative description of the otherwise extremely thoroughly studied chemotaxis pathway. The rates of exchange at the cluster appear to match the signaling functions of the chemotaxis proteins, extending our view of the pathway as an evolutionarily optimized system (15, 43, 44).

Methods

Bacterial Strains and Plasmids. Strains VS102 and VS116 were derived from *E. coli* K-12 strain RP437 (45). VS102 carries a deletion of the anti-sigma factor *flgM*, negative regulator of class III flagellar and chemotaxis genes, and consequently overexpresses all chemotaxis proteins by ≈6-fold (15). VS116 is deleted for *flhC*, a master activator of flagellar and chemotaxis gene expression and does not express any chemotaxis proteins (46). Both strains were transformed with plasmids encoding fusions of chemotaxis proteins to enhanced yellow fluorescent protein (YFP). Fusions were expressed under control of a pTrc promoter (47), which is inducible by isopropyl-β-D-thiogalactopyranoside (IPTG). Optimal levels of induction for individual constructs were determined by a visual microscopic examination. All plasmids and corresponding induction levels are summarized in Table S1.

Cell Growth and Preparation. Overnight cultures were grown at 30°C in 5 ml of tryptone broth (TB) [10 g/liter tryptone and 5 g/liter NaCl (pH 7.0)] containing 100 μg/ml ampicillin. Daily cultures were prepared by diluting the overnight culture 1:100 in 10 ml of TB containing 100 μg/ml ampicillin and the appropriate concentration of IPTG (Table S1). These cultures were grown in a Unitron rotary shaker (Infors AG) at 34°C and 275 rpm to $OD_{600} \approx 0.45–0.5$, washed once in tethering buffer [10 mM KH_2PO_4/K_2HPO_4, 0.1 mM EDTA, 10 mM sodium lactate, 67 mM NaCl, and 1 μM methionine (pH 7.0)] and resuspended in 10 ml of tethering buffer. The cells were incubated at 4°C for at least 1 h to stop growth and protein production and were immobilized for FRAP experiments on (poly)L-lysin-coated coverslips for 5 min.

FRAP Analyses. Measurements were performed on a laser-scanning confocal microscope (Leica TCS SP2) equipped with a 20-mW argon laser and a FRAP software module. Cells expressing YFP fusion proteins were visualized through a 63× oil objective, using a 514-nm laser line and a YFP emission channel (525–650 nm) with a ×32 zoom magnification. All measurements were performed at 20°C. Cells with similar levels of fluorescence were selected for bleaching experiments, and subsequent image analysis confirmed that the difference in fluorescence among cells expressing different fusions was less than threefold. Fluorescence of the (polar) region of interest (ROI) was bleached with two 0.336-s laser scans at 50% laser intensity; prebleach image and postbleach image sequences were acquired with 1–5% laser intensity. Postbleach image series consisted of 10 images taken every 0.336 s, 10 images taken every 3 s, and 5–40 images taken every 30 s, using bidirectional scanning.

Image Analyses. Images (512 × 512 pixels) of a FRAP sequence were recorded by using Leica Confocal software, Version 2.61, and were subsequently analyzed by using ImageJ software, Version 1.34l (W. Rasband, National Institutes of Health, Bethesda, MD; http://rsb.info.nih.gov/ij). Fluorescence intensity of the polar ROI (defined as 52 pixels) was measured automatically in image sequences, using a custom-written ImageJ plug-in. The length of this region was ≈23% of the average cell length, ≈230 pixels, or 3.3 μm. We compensated gradual bleaching of the image during scanning by normalizing the fluorescence of the ROI to the integral fluorescence of the entire cell in the same image. To facilitate comparison of multiple experiments with different bleaching depth and different cluster intensity, the relative fluorescence intensity of the ROI in the image sequence was normalized again to the relative ROI intensity before bleaching. Data were subsequently processed by using KaleidaGraph software, Version 3.6 (Synergy Software). To determine the bleach profile (Fig. 2), fluorescence intensity was measured by using ImageJ within a stripe drawn over the entire cell length. The resulting profile was smoothed by using *Smooth* function of KaleidaGraph.

Data fitting. Fluorescence recovery due to diffusional exchange in strain VS116 was approximated as

$$I(t) = \frac{F_0 + F_\infty \left(\frac{t}{t_{1/2}}\right)^\alpha}{1 + \left(\frac{t}{t_{1/2}}\right)^\alpha} \quad [1]$$

where F_0 is relative fluorescence intensity after bleaching, F_∞ is intensity after recovery, $t_{1/2}$ is the half-time of recovery, and α is the factor accounting for the anomalous diffusion (23).

Biphasic fluorescence recovery in presence of cluster association (strain VS102) was treated as a combination of the purely diffusional equilibration and protein exchange at the cluster, with the latter being approximated by an exponential decay with a characteristic time τ_{obs} (31, 32),

$$I(t) = \frac{F_0 + F_\infty \left(\frac{t}{t_{1/2}}\right)^\alpha}{1 + \left(\frac{t}{t_{1/2}}\right)^\alpha} + C\left(1 - e^{-\left[\frac{t}{\tau_{obs}}\right]}\right) \quad [2]$$

with $F = F_\infty - F_0$ and C being relative steady-state concentrations of free and cluster-bound fluorescent protein, respectively. Such separation is valid as long as the diffusional equilibration is much faster, and the pseudo-first-order on-rate constant $^*k_{on}$ of protein binding at the cluster is not diffusion-limited, i.e., $(^*k_{on}w^2/D) \ll 1$, where w is the size of the bleached spot (31); this condition is fulfilled for all proteins except CheY (Table 1). Values for $t_{1/2}$ and α that have been estimated from the VS116 data were substituted into Eq. **2**. As shown in *SI Text*, the value of τ_{obs} can be used to estimate the off-rate constant of protein dissociation from the cluster as $k_{off} \approx \tau_{obs}^{-1}$.

Numerical Simulation of Anomalous Diffusion and Cluster Binding. VPLAN software package (48) was used to estimate the values of diffusion coefficients and binding rates by fitting the data to the reaction-diffusion equations as described in *SI Text*. Even in absence of clustering, fluorescence recovery could not be fitted well by simple diffusion, indicating anomalous protein diffusion in the cell. Such anomalous diffusion was modeled by using a concept of ghost particles (28–30), which mimic virtual reaction partners and artificially delay diffusion of proteins. The values of diffusion parameters were estimated in absence of clustering. For CheY-YFP, these values were used to estimate the value for k_{off} in presence of clustering. Parameter estimation was performed by discretizing the spatial coordinate of the model into 100 equally spaced grid points; estimation outcome was the same

with slightly smaller and with much larger numbers of distributed grid points. Discretization of the spatial derivatives was done according to the finite difference method and initial values were set in accordance with the measured data. See *SI Methods* for details.

ACKNOWLEDGMENTS. We thank Stefan Körkel (Humboldt-Universität zu Berlin, Berlin, Germany) and Hans-Georg Bock (University of Utah, Salt Lake City) for providing the VPLAN package for parameter estimation, Nora Rieber for the help with image data analysis, and John S. Parkinson for critical reading of the manuscript. This work was supported by Deutsche Forschungsgemeinschaft Grants SO 421/3–1 and SO 421/6–1 (to V.S.) and LE 1415/5–1 (to D.L.).

1. Bourret RB, Stock AM (2002) Molecular information processing: Lessons from bacterial chemotaxis. *J Biol Chem* 277:9625–9628.
2. Sourjik V (2004) Receptor clustering and signal processing in *E. coli* chemotaxis. *Trends Microbiol* 12:569–576.
3. Wadhams GH, Armitage JP (2004) Making sense of it all: Bacterial chemotaxis. *Nat Rev Mol Cell Biol* 5:1024–1037.
4. Sourjik V, Berg HC (2004) Functional interactions between receptors in bacterial chemotaxis. *Nature* 428:437–441.
5. Ames P, Studdert CA, Reiser RH, Parkinson JS (2002) Collaborative signaling by mixed chemoreceptor teams in *Escherichia coli*. *Proc Natl Acad Sci USA* 99:7060–7065.
6. Jasuja R, Keyoung J, Reid GP, Trentham DR, Khan S (1999) Chemotactic responses of *Escherichia coli* to small jumps of photoreleased L-aspartate. *Biophys J* 76:1706–1719.
7. Segall JE, Block SM, Berg HC (1986) Temporal comparisons in bacterial chemotaxis. *Proc Natl Acad Sci USA* 83:8987–8991.
8. Segall JE, Manson MD, Berg HC (1982) Signal processing times in bacterial chemotaxis. *Nature* 296:855–857.
9. Sourjik V, Berg HC (2002) Binding of the *Escherichia coli* response regulator CheY to its target measured *in vivo* by fluorescence resonance energy transfer. *Proc Natl Acad Sci USA* 99:12669–12674.
10. Berg HC, Tedesco PM (1975) Transient response to chemotactic stimuli in *Escherichia coli*. *Proc Natl Acad Sci USA* 72:3235–3239.
11. Spudich JL, Koshland DE, Jr (1975) Quantitation of the sensory response in bacterial chemotaxis. *Proc Natl Acad Sci USA* 72:710–713.
12. Li M, Hazelbauer GL (2004) Cellular stoichiometry of the components of the chemotaxis signaling complex. *J Bacteriol* 186:3687–3694.
13. Morton-Firth CJ, Shimizu TS, Bray D (1999) A free-energy-based stochastic simulation of the Tar receptor complex. *J Mol Biol* 286:1059–1074.
14. Barkai N, Leibler S (1997) Robustness in simple biochemical networks. *Nature* 387:913–917.
15. Kollmann M, Løvdok L, Bartholome K, Timmer J, Sourjik V (2005) Design principles of a bacterial signalling network. *Nature* 438:504–507.
16. Mello BA, Tu Y (2003) Perfect and near-perfect adaptation in a model of bacterial chemotaxis. *Biophys J* 84:2943–2956.
17. Shimizu TS, Aksenov SV, Bray D (2003) A spatially extended stochastic model of the bacterial chemotaxis signalling pathway. *J Mol Biol* 329:291–309.
18. Lipkow K (2006) Changing cellular location of CheZ predicted by molecular simulations. *PLoS Comput Biol* 2:e39.
19. Golding I, Cox EC (2006) Physical nature of bacterial cytoplasm. *Phys Rev Lett* 96:098102.
20. Andrews SS, Bray D (2004) Stochastic simulation of chemical reactions with spatial resolution and single molecule detail. *Phys Biol* 1:137–151.
21. Lipkow K, Andrews SS, Bray D (2005) Simulated diffusion of phosphorylated CheY through the cytoplasm of *Escherichia coli*. *J Bacteriol* 187:45–53.
22. Slepchenko BM, Schaff JC, Macara I, Loew LM (2003) Quantitative cell biology with the Virtual Cell. *Trends Cell Biol* 13:570–576.
23. Feder TJ, Brust-Mascher I, Slattery JP, Baird B, Webb WW (1996) Constrained diffusion or immobile fraction on cell surfaces: A new interpretation. *Biophys J* 70:2767–2773.
24. Elowitz MB, Surette MG, Wolf PE, Stock JB, Leibler S (1999) Protein mobility in the cytoplasm of *Escherichia coli*. *J Bacteriol* 181:197–203.
25. Konopka MC, Shkel IA, Cayley S, Record MT, Weisshaar JC (2006) Crowding and confinement effects on protein diffusion *in vivo*. *J Bacteriol* 188:6115–6123.
26. Banks DS, Fradin C (2005) Anomalous diffusion of proteins due to molecular crowding. *Biophys J* 89:2960–2971.
27. Weiss M, Elsner M, Kartberg F, Nilsson T (2004) Anomalous subdiffusion is a measure for cytoplasmic crowding in living cells. *Biophys J* 87:3518–3524.
28. Nguyen HD, Hall CK (2005) Kinetics of fibril formation by polyalanine peptides. *J Biol Chem* 280:9074–9082.
29. Tepper HL, Voth GA (2005) Protons may leak through pure lipid bilayers via a concerted mechanism. *Biophys J* 88:3095–3108.
30. Vliegenthart GA, van der Schoot P (2003) Kinetics of depletion interactions. *Europhys Lett* 62:600–606.
31. Sprague BL, Pego RL, Stavreva DA, McNally JG (2004) Analysis of binding reactions by fluorescence recovery after photobleaching. *Biophys J* 86:3473–3495.
32. Bulinski JC, Odde DJ, Howell BJ, Salmon TD, Waterman-Storer CM (2001) Rapid dynamics of the microtubule binding of ensconsin *in vivo*. *J Cell Sci* 114:3885–3897.
33. Deich J, Judd EM, McAdams HH, Moerner WE (2004) Visualization of the movement of single histidine kinase molecules in live *Caulobacter* cells. *Proc Natl Acad Sci USA* 101:15921–15926.
34. Kim SY, Gitai Z, Kinkhabwala A, Shapiro L, Moerner WE (2006) Single molecules of the bacterial actin MreB undergo directed treadmilling motion in *Caulobacter crescentus*. *Proc Natl Acad Sci USA* 103:10929–10934.
35. Leake MC, *et al.* (2006) Stoichiometry and turnover in single, functioning membrane protein complexes. *Nature* 443:355–358.
36. Cluzel P, Surette M, Leibler S (2000) An ultrasensitive bacterial motor revealed by monitoring signaling proteins in single cells. *Science* 287:1652–1655.
37. Gegner JA, Graham DR, Roth AF, Dahlquist FW (1992) Assembly of an MCP receptor, CheW, and kinase CheA complex in the bacterial chemotaxis signal transduction pathway. *Cell* 70:975–982.
38. Vaknin A, Berg HC (2004) Single-cell FRET imaging of phosphatase activity in the *Escherichia coli* chemotaxis system. *Proc Natl Acad Sci USA* 101:17072–17077.
39. Berg HC, Brown DA (1972) Chemotaxis in *Escherichia coli* analysed by three-dimensional tracking. *Nature* 239:500–504.
40. Levin MD, Shimizu TS, Bray D (2002) Binding and diffusion of CheR molecules within a cluster of membrane receptors. *Biophys J* 82:1809–1817.
41. Korobkova E, Emonet T, Vilar JM, Shimizu TS, Cluzel P (2004) From molecular noise to behavioural variability in a single bacterium. *Nature* 428:574–578.
42. Li G, Weis RM (2000) Covalent modification regulates ligand binding to receptor complexes in the chemosensory system of *Escherichia coli*. *Cell* 100:357–365.
43. Berg HC, Purcell EM (1977) Physics of chemoreception. *Biophys J* 20:193–219.
44. Andrews BW, Yi TM, Iglesias PA (2006) Optimal noise filtering in the chemotactic response of *Escherichia coli*. *PLoS Comput Biol* 2:e154.
45. Parkinson JS, Houts SE (1982) Isolation and behavior of *Escherichia coli* deletion mutants lacking chemotaxis functions. *J Bacteriol* 151:106–113.
46. Kentner D, Thiem S, Hildenbeutel M, Sourjik V (2006) Determinants of chemoreceptor cluster formation in *Escherichia coli*. *Mol Microbiol* 61:407–417.
47. Amann E, Ochs B, Abel KJ (1988) Tightly regulated *tac* promoter vectors useful for the expression of unfused and fused proteins in *Escherichia coli*. *Gene* 69:301–315.
48. Körkel S, Kostina E, Bock HG, Schlöder JP (2004) Numerical methods for optimal control problems in design of robust optimal experiments for nonlinear dynamic processes. *Optim Method Softw* 19:327–338.